Int J Adv Manuf Technol (2017) 93:975–991
DOI 10.1007/s00170-017-0566-9

ORIGINAL ARTICLE

Study of surface roughness and cutting forces using ANN, RSM, and ANOVA in turning of Ti-6Al-4V under cryogenic jets applied at flank and rake faces of coated WC tool

Mozammel Mia[1] · **Md Awal Khan**[2] · **Nikhil Ranjan Dhar**[3]

Received: 26 January 2017 / Accepted: 15 May 2017 / Published online: 1 June 2017

Abstract This paper presents the analysis of average surface roughness, cutting force, and feed force in turning of difficult-to-machine Ti-6Al-4V alloy by experimental investigation and performance modeling. Based on knowledge of the literature, to pacify the elevated temperature in machining Ti-6Al-4V and to ensure a clean environment, the experiments are carried out in cryogenic (liquid nitrogen) condition by following the Taguchi L_{18} mixed-level orthogonal array. Afterward, the models of responses have been formulated by the response surface methodology (RSM) and artificial neural network (ANN). The higher values of correlation coefficient (≥96%) and lower values of error determined the adequacy of the developed models. Comparative study of both models revealed that the RSM-based model revealed greater accuracy for the testing data and hence recommended. Analysis of variance (ANOVA) determined the effects of cutting speed, feed rate, and insert configuration on the quality characteristics. The results revealed that a cutting speed not exceeding 110 m/min is likely to generate favorable machining responses. In addition, the higher feed rate was found to ensure better machining performances. Moreover, the desirability-based multi-response optimization determined that a cutting speed of 78 m/min, a feed rate of 0.16 mm/rev, and use of the SNMM tool insert are capable of minimizing surface roughness at 1.05 μm, main cutting force at 315 N, and feed force at 208 N.

Keywords Surface roughness · Machining forces · Cryogenic liquid nitrogen · Artificial neural network · Response surface methodology

✉ Mozammel Mia
arif_ipe@yahoo.com; mozammel.mpe@aust.edu; mozammelmiaipe@gmail.com

Md Awal Khan
awalsetu@yahoo.co.uk

Nikhil Ranjan Dhar
nrdhar@ipe.buet.ac.bd

[1] Mechanical and Production Engineering, Ahsanullah University of Science and Technology, Dhaka, Bangladesh

[2] Industrial and Production Engineering, Military Institute of Science and Technology, Dhaka, Bangladesh

[3] Industrial and Production Engineering, Bangladesh University of Engineering and Technology, Dhaka, Bangladesh

1 Introduction

Ti-6Al-4V has been extensively used in many critical engineering areas, typically in load-carrying parts, chemical plant, and aerospace industries due to its versatile properties [1]. This acceptability of Ti alloy is mainly accredited to its load taking capability at elevated temperature and high specific strength. However, at the same time, it is appraised as a difficult-to-machine material owing to the adversities faced during machining which are caused by the low Young's modulus, poor thermal conductivity, and high chemical reactivity [2, 3]. As a result, the performances get affected and the machining cost is increased. Researchers are seeking a way to economically machine Ti-6Al-4V and, furthermore, trying to control the machining process. Since Young's modulus is a material's inherent property and cannot be changed, the focus of researchers is to increase thermal (heat) dissipation from the cutting zone. In addition, inertness is required to hinder the chemical reactivity during the cutting.

Though the use of conventional cutting fluid can ensure thermal cooling and lubrication, it violates the principle of sustainable manufacturing due to its detrimental effects on

the machine operator's health and natural environment. In addition, it is proved as counter-productive due to higher cost associated with the huge amount of circulated fluid. In this regard, the implementation of liquid nitrogen (cryogenic) is deemed as an alternative sustainable solution [4]. The liquid state of N_2 (very low temperature), its chemical inertness, and, most significantly, its environmental friendliness offer this green technology as a problem solver for the aforementioned adversities.

Researchers have reported the use of various coolant technologies for attaining amiable machinability of titanium alloy. Notable coolant technologies include high-pressure coolant, minimum-quantity coolant, and compressed-air and cryogenic cooling [5–8]. It is reported that machining of Ti alloy is possible by pacifying the temperature-oriented effects under cryogenic application [9]. In support, Sun et al. [10] used cryogenic compressed air and found reduced cutting temperature which extended tool life and reduced cutting force. Vazquez et al. [11] analyzed the superiority of MQL over dry and flood cutting in respect of surface finish and tool wear in micro-milling. Moura et al. [12] evaluated the performance of solid lubricant mixed with fluid in machining of Ti alloy in respect of surface roughness, force, and temperature. da Silva et al. [13] examined tool wear in high-pressure-coolant-assisted turning. Xie et al. [14] experimentally investigated the temperature and force in turning using a specially designed grooved tool. Su et al. [1] investigated tool wear behavior under different environments in high-speed milling.

Effective control of machining is executed by modeling of the performances prior to actual machining. The predictive models of the quality characteristics forecast the outcome of any machining well before it happens. As a result, the machining phenomena can be molded accordingly in favor of higher productivity. Besides, the mathematical model aids in understanding the relation of a quality response with the influential parameters.

Conventional (statistical regression) and non-conventional (artificial intelligence) modeling techniques are proved to be successful for various machining phenomena, although that particular technique may not bring the best result for another case [15]. For instance, Hasçalık and Çaydaş [16] employed the Taguchi technique to optimize surface roughness and tool life for turning of Ti-6Al-4V. A surface roughness prediction model was developed by Zain et al. [15] by employing an artificial neural network (ANN), and the model showed good agreement between the actual and predicted surface roughness. Hashmi et al. [17] developed a response surface methodology (RSM)-based optimization model for minimum surface roughness in milling of Ti-6Al-4V. Moufki et al. [18] analytically derived cutting force for peripheral milling of Ti-6Al-4V. Ramesh et al. [19] analyzed surface roughness using the RSM and developed a predictive model while machining Ti alloy. Mia et al. [20, 21] in their studies conducted modeling of different response parameters by using ANN, support vector regression, the Taguchi S/N ratio, and the Grey-Taguchi method with good accuracy between the modeled results and actual machining data. However, their studies, though focused on machining of Ti-6Al-4V alloy, were under the application of high-pressure oil dual jets.

The presented work, in the literature, are either in the form of experimental investigation, to evaluate the effects of any particular factor or change on the responses, or in the form of model development and validation for Ti-6Al-4V. However, the studies revealed the existence of very few predictive models of the cutting forces in the turning process. On the contrary, some studies have been conducted for modeling of surface roughness in machining of Ti-6Al-4V. Furthermore, the congenial effects of cryogenic environment are well established [4, 22] and implemented extensively in machining of difficult-to-cut alloys. Yet, no such model exists that can predict main cutting force, feed force, and surface roughness for a range of values of cutting speed and feed rate in turning of Ti-6Al-4V using two different tool inserts under the application of liquid nitrogen. More to it, the performance of two commercial coated carbide inserts (SNMM, SNMG) needs to be evaluated in respect of favorable machinability.

Therefore, the study of investigation and formulation of the predictive models of surface roughness and cutting forces in turning under cryogenic machining condition is inevitable. For that objective, in this study, the effects of cutting speed and feed rate have been analyzed by using 2D and 3D graphical plots and analysis of variance. Furthermore, the response surface method and artificial neural network have been employed to design the predictive models of main cutting force, feed force, and surface roughness in turning of Ti-6Al-4V alloy using two widely used tool inserts, i.e., SNMM and SNMG. Finally, the performance of the developed models has been checked by error analysis.

2 Methodology

2.1 Experimental conditions

The straight turning of Ti-6Al-4V (grade 5) having a diameter of 100 mm and length of 400 mm has been carried out by a powerful center lathe (7.5 kW, China) by using coated carbide inserts of two different ISO specifications, namely SNMG 120408 and SNMM 120408. The chemical composition of Ti-6Al-4V is shown in Table 1. Numerous studies are available in the literature wherein the conventional overflow-type liquid cutting fluid has been used to pacify the elevated temperature that prevails in the tool-work interface during turning of Ti-6Al-4V. It is further noticeable that in most of the cases, that coolant is ineffective in reducing the temperature. As alternative cooling technology, cryogenic cooling is

Table 1 Chemical composition of Ti-6Al-4V

	Element							
	Al	V	Fe	O	C	N	H	Ti
%wt	6.34	4.12	0.04	0.194	0.014	0.009	0.0023	Balance

recommended. Based on this recommendation, in this study, the cryogenic condition (by liquid nitrogen at –196 °C) is applied. In machining such a difficult-to-cut material, friction-induced heat generation occurs not only at the tool's rake surface but also at the principal flank face. Keeping this in mind, the liquid nitrogen jets were impinged at the rake and principal flank face of the insert by using a specially designed nozzle applicator as shown in Fig. 1. The liquid nitrogen jet applied at the rake surface (chip-tool interface) was oriented at 70° with the normal of the rake face and along the auxiliary cutting edge of the tool. At the same time, the jet applied at the flank surface (tool-work interface) was making an angle of 15° with the principal cutting edge [23, 24]. The experimental conditions are listed in Table 2.

The depth of cut was kept constant at 1.0 mm. The cutting speed, feed rate, and tool insert configuration have been considered as the input variables and diffused into levels as shown in Table 3. The experimental layout has been oriented by following a Taguchi L_{18} mixed-level orthogonal array-based experimental design. Surface roughness was measured by a Talysurf (Surtronic 3+) roughness checker; main cutting and feed force were monitored by a 3D dynamometer (Kistler) equipped with a data acquisition system. The photographic view of the experimental setup is shown in Fig. 2. During the recording of these responses, three replicates were taken corresponding to each machining run, and afterward, the mean of these three values was obtained for further analysis. The recorded forces and surface roughness are listed in Table 4. Afterward, these data are used for the formulation of the artificial neural network predictive model and response surface methodology-based predictive, mathematical, and optimization model.

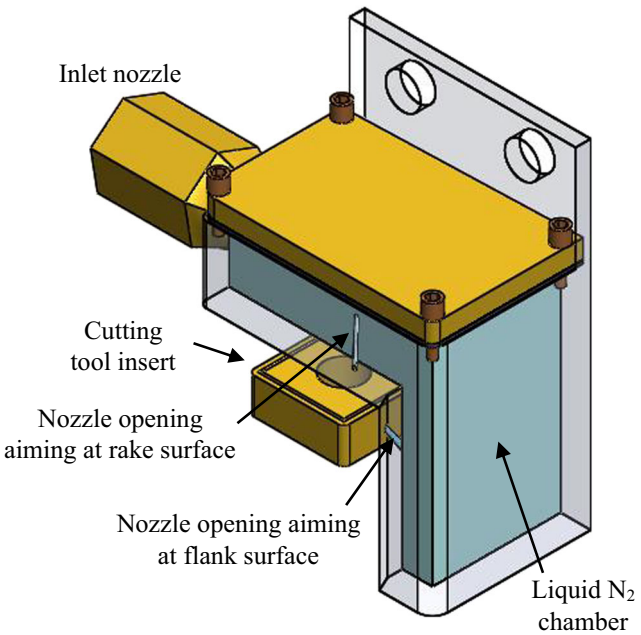

Fig. 1 Schematic of nozzle system for simultaneous applications of liquid nitrogen at the rake surface and principal flank surface of cutting tool insert

2.2 Artificial neural network

A feed forward back-propagation multi-layer neural network with 3-n-1 architecture has been used, separately, for each response. The used structure, as shown in Fig. 3, has three input neurons (corresponding to the cutting speed, feed rate, and cutting tool insert) and possess n number of neurons (determined by the accuracy level) and one output neuron (main cutting force or feed force or surface roughness). Basically, this type of neural network algorithm works by following the ten steps [25] listed in Table 5.

The ANN models of forces and surface roughness have been trained by using the Bayesian regularization "trainbr" of the MATLAB R2015a "nnstart" wizard. Bayesian regularization [26] can handle imprecise data by solving problems regarding overfitting and underfitting. Moreover, the distribution of weights and biases to the neurons is random, and after an analysis, the optimum weights are assigned [27]. In the hidden layer, the hyperbolic tangent sigmoid function "tansig" and, in the output layer, the pure linear function "purelin" have been employed based on the study of Ezugwu et al. [28]. During training of models, the error function "mean square error" (MSE) and, during testing of the models, the "mean absolute percentage error" (MAPE) were employed. The error functions are defined in Eqs. 1 and 2.

$$\mathrm{MSE} = \frac{1}{N}\sum_{n=1}^{N}(\mathrm{Actual}-\mathrm{Predicted})^2 \tag{1}$$

$$\mathrm{MAPE} = \frac{1}{N}\sum_{n=1}^{N}\left(\frac{|\mathrm{Actual}-\mathrm{Predicted}|}{\mathrm{Actual}}\right)\times 100 \tag{2}$$

It is a challenge to develop an effective model with few numbers of experimental data. Nonetheless, it is essential and therefore can determine the ability of a particular method in formulating a model. Among the 18 data sets in Table 4, randomly selected 13 sets have been used to construct models and the other 5 sets were employed for the validation of the developed ANN model. Note that as mentioned earlier, the model is "3-n-1"; thereby, for each response (i.e., surface roughness, feed force, and main cutting force), this training and testing ratio (=13:5) remains valid.

Table 2 Experimental conditions

Category	Specification
Machine tool	Lathe; origin, China; power, 7.5 kW
Material	Ti-6Al-4V; grade, 5; phase, α + β; hardness, 35–40 Rockwell C; density, 4.43 g/cm^3; heat conductivity, 7 W/mK; yield strength, 950 MPa; tension strength, 1050 MPa; Young's modulus, 110 N/mm^2; elongation, 8%
Cutting tool	SNMG 120408 (chip breaker at double side); SNMM 120408 (chip breaker at single side); material, WC; coating, CVD Ti(C,N) + Al_2O_3 + TiN; shape, square; clearance angle, 0°; rake angle, 0°; effective cutting edge length, 11.91 mm; insert thickness, 4.76 mm; nose radius, 0.8 mm
Tool holder	PSBNR 2525 M12
Cutting parameters	Cutting speed and feed rate, variable; depth of cut, 1.0 mm
Machining length	200 mm per experimental run
Cutting tool condition	New tool in each machining run
Cutting environment	Cryogenic condition by liquid nitrogen (temperature, −196 °C)

2.3 Response surface methodology

The RSM is a conventional statistical tool to formulate an approximate mathematical relationship, for modeling, simulation, and optimization, of the dependent variables (herein main cutting force, feed force, and surface roughness) in terms of the independent variables (herein the cutting speed, feed rate, and tool insert) [29, 30]. The RSM covers the response(s) of a system (i.e., machining system) for a range of factor levels and further deals with defining a region corresponding to the optimum solution or near-optimum solution. As a course of action, the response can be mathematically related with the factors by using first-order or second-order polynomial equations. For a complex system like machining wherein multiple factors influence the outcome and there exist mutual interactions, the pure linear system hardly reflects the actual machining behavior. In this perspective, the use of the quadratic response function as shown in Eq. 3 is deemed more appropriate to express the relevant relation.

$$X = \beta_o + \sum_{i=1}^{k} \beta_i x_i + \sum_{i=1}^{k} \beta_{ii} {x_i}^2 + \sum\sum_{i<j} \beta_{ij} x_i x_j + \varepsilon \quad (3)$$

where X is the dependent variable; β_o is the fixed term; β_i, β_{ii}, β_{ij} are the coefficients of linear, quadratic, and cross-product terms, respectively; and x_i is the input variable.

This general equation can be presented as Eq. 4 wherein the symbols of the current study are used.

Table 3 Input variables and distribution of levels

Variables	Level 1	Level 2	Level 3
Cutting speed, V_c (m/min)	78	112	156
Feed rate, f (mm/rev)	0.12	0.14	0.16
Tool insert, T	SNMM	SNMG	–

$$Y = C + Vc + f + Vc^2 + f^2 + Vc \times f \quad (4)$$

Here, Y indicates the response parameter (i.e., P_z, P_x, and R_a) and C is the constant term. Note that the independent variable cutting tool (T) insert is a categorical variable and therefore is not included in Eq. 4; rather, two forms of Eq. 4 respective to SNMM and SNMG are constructed.

Associated with the RSM is the statistical analysis of variance (ANOVA). The influences of the individual factor and interactions among factors on the responses are determined by the ANOVA. Furthermore, it assists in determining the statistical significance [31].

Optimization by the desirability method includes the use of an objective function, also called the desirability function, denoted by $D(X)$. $D(X)$ comprises multiple desirability values (i.e., d_i). Each desirability ranges from the least to the most which in turn possesses the numerical value 0 to 1. Presumably, the highest combined desirability, which is computed by taking the geometric means of all the desirability functions, represents the optimum responses for an optimum parameter setting. The combined objective function is shown in Eq. 5.

$$D = (d_1 \times d_2 \times \ldots \times d_n)^{1/n} = \left(\prod_{i=1}^{n} d_i \right)^{1/n} \quad (5)$$

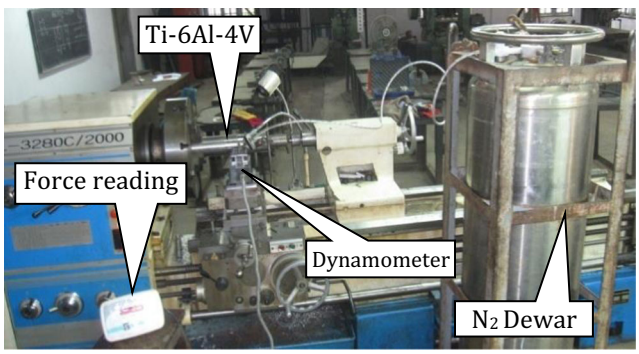

Fig. 2 Experimental setup

Table 4 Taguchi L_{18} mixed-level orthogonal array and machining characteristics

Exp. runs	Input variables			Responses		
	V_c (m/min)	f (mm/rev)	T	P_z(N)	P_x(N)	R_a(N)
1	78	0.12	SNMG	370	229	2.65
2	78	0.12	SNMM	330	218	1.12
3	78	0.14	SNMG	370	229	4.28
4	78	0.14	SNMM	330	218	1.22
5	78	0.16	SNMG	320	198	3.66
6	78	0.16	SNMM	320	211	1.1
7	112	0.12	SNMG	390	242	2.78
8	112	0.12	SNMM	370	244	1.52
9	112	0.14	SNMG	380	236	2.89
10	112	0.14	SNMM	380	251	1.59
11	112	0.16	SNMG	350	217	2.9
12	112	0.16	SNMM	360	238	1.4
13	156	0.12	SNMG	400	248	2.91
14	156	0.12	SNMM	400	264	3.54
15	156	0.14	SNMG	410	254	3.2
16	156	0.14	SNMM	400	264	3.74
17	156	0.16	SNMG	390	242	3.21
18	156	0.16	SNMM	390	257	3.48

The tentative goals for optimization are to maximize, minimize, reach a target, within range, none (applicable for responses), and meet an exact value (applicable for factors only). This study focuses on the "minimization" goal for all the responses and concurrently applies "within range" for the factors. Therefore, the following relations are applicable:

- Minimum:
  - $d_i = 1$ if response < low value
  - $1 \le d_i \le 1$ as response varies from low to high
  - $d_i = 0$ if response > high value
- Range:
  - $d_i = 0$ if response < low value
  - $d_i = 1$ as response varies from low to high
  - $d_i = 0$ if response > high value

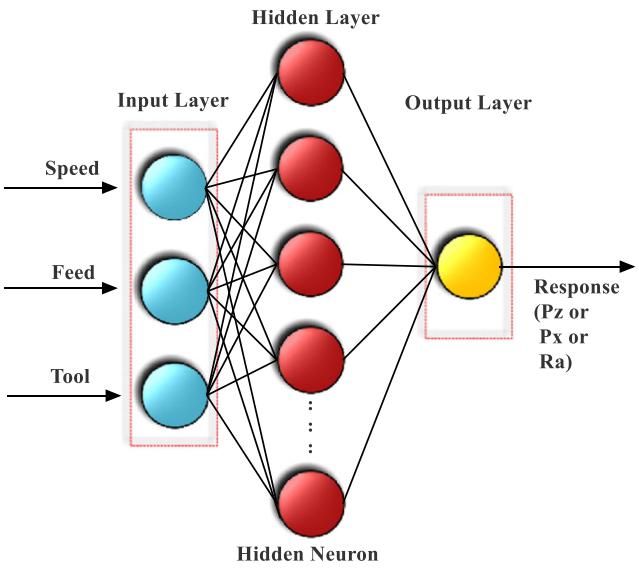

Fig. 3 ANN architecture for three inputs and one output

3 Results and discussion

3.1 Probability distribution of machining data

Prior to using the collected machining response data, they have been analyzed with the appropriate probability distribution function so that it is ensured that the data are usable. Generally, any system is likely to generate data that are normally distributed; therefore, it is highly imperative that for each of the responses (i.e., main cutting force, feed force, and average surface roughness), the collected data are checked for the assumption of normal distribution.

Empirical cumulative distribution (ECD) is such a statistical tool that analyzes a parameter for a specific probability distribution function [5, 31]. Since this study concerns the normal distribution function, herein the collected data are plotted for ECD in Fig. 4 in association with normal distribution. Herein, the x-axis represents the collected data of cutting forces and surface roughness while the y-axis indicates the percentile. Figure 4a includes the ECD of main cutting force and feed force whereas Fig. 4b shows that of surface roughness. In all these plots, the stepped (stair like) lines indicate a gradual progression of both the data value and percentage value of the actual data. On the contrary, the smooth curve passing through the stepped line is the representative of the normal distribution function.

It is appreciable that main cutting force (P_z) and feed force (P_x) are reasonably aligning with the normal distribution function. Though the surface roughness parameter is showing little discrepancy in aligning with the normal distribution curve, it is acceptable to further process for the mathematical modeling, prediction of performance parameters, and optimization results. At the same time, it becomes important to investigate the reason for this variance. To be exact, the means of P_z, P_x, and R_a are 370 N, 236.7 N, and 2.62 μm, respectively, and the standard deviations are 29.1 N, 18.8 N, and 1.02 μm, correspondingly. Consequently, the coefficient of variation (C_v) value, which is the representative of the data dispersion, computed by taking the ratio of the standard deviation with respect to the mean value, stands at 7.86, 7.94, and 39.13%, respectively, for main cutting force, feed force, and average surface

Table 5 Steps for the feed forward back-propagation neural network

Step	Description	For this study
1	Number of hidden layers to be used	1
2	Input and output neuron numbers to be selected	3 and 1, respectively
3	Training function selection	Bayesian regularization
4	Assigning weights to the links	Smaller is better
5	Outputs of hidden and output layers to be calculated $\text{out}_i = f(\text{net}_1) = f\left(\sum_{w_{ij}} \text{out}_j + \theta_1\right)$ Here out_i represents the output of the ith neuron of the said layer whereas out_j stands for the output of the jth neuron of the preceding layer.	f is the tan sigmoid function $f(\text{net}_1) = \frac{2}{1+e^{-2n}} - 1$
6	Computing the output and comparison with the expected output. Computation of error (desired value − actual value) and root-mean-square error	$E_p = \frac{1}{2}\sum(t_{pj} - d_{pj})^2$ Here E_p represents the error for the pth vector and t_{pj} and d_{pj} stand for the actual and desired output values, respectively.
7	Evaluating the errors in the hidden layers and back-propagation for the hidden and output layers. Adjustment of weights accordingly	For output neurons, error— $\delta_{pi} = (t_{pi} - d_{pi})d_{pi}(1 - d_{pi})$ For hidden neurons, error— $\delta_{pi} = (t_{pi} - d_{pi})d_{pi}\sum \delta_{pi}W_{ki}$ For weight adjustment— $\Delta W_{ji}(n=1) = \eta(\delta_{pi}d_{pi}) = \alpha\Delta W_{ji}(n)$ Here η represents the learning rate parameter.
8	Iterations continued until the predefined criteria are met.	
9	After stopping of iterations, the ultimate weight values attached with the hidden and output layers are noted.	
10	Validating the neural network model with the testing data. In this stage, the prediction error should be sufficiently low. Otherwise, the back-propagation model is again run with a new set of the aforementioned parameters.	

roughness in turning of Ti-6Al-4V alloy under cryogenic condition. This low value of the coefficient of variation (of P_z and P_x) provides the acceptability of using these data. However, the high value of the coefficient of variation of R_a can be justified if one or more factor(s) influenced the responses to be changed significantly. This clarification is provided in Sections 3.2 and 3.3.

3.2 Analysis of variance

As mentioned earlier, the influence of each factor on the individual response is determined by using analysis of variance (ANOVA). The ANOVA operates based on parameters, namely the sum of squares (SS), P value, and F statistics. The SS indicates the deviation from the mean, which is derived from that source (factor); the P value represents the statistical significance to a confidence interval of 95% (i.e., significance level $\alpha = 0.05$); if the P value is lower than α, then that factor (or source) is significant; lastly, the F statistics, which is derived by dividing the term MS of a factor with MS of error, tells the relative importance of the factors [30, 32].

Table 6 shows the ANOVA for main cutting force. A study based on the aforementioned parameters reveals that the highest variation in main cutting force comes from the cutting

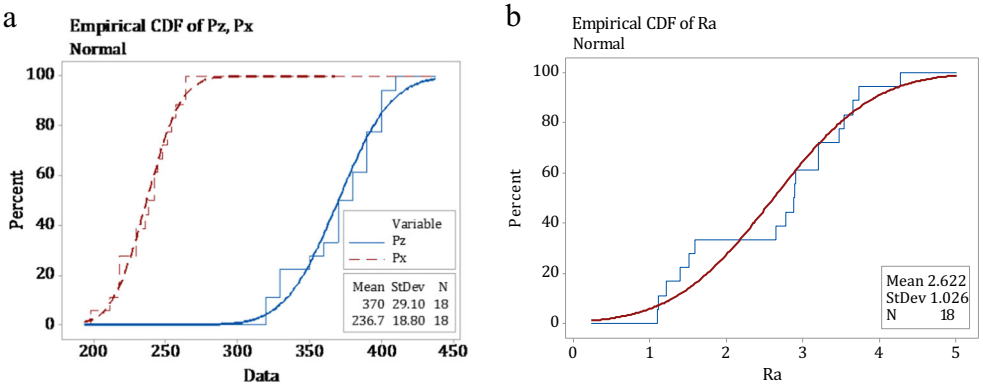

Fig. 4 Empirical cumulative distribution functions of **a** cutting forces and **b** surface roughness

Table 6 ANOVA for main cutting force

Source	DF	Adj. SS	Adj. MS	*F*	*P*	Remark
Cutting tool	1	555.6	555.6	4.23	0.062	Not significant
Cutting speed	2	10,233.3	5116.7	38.92	0.000	Significant
Feed rate	2	2033.3	1016.7	7.73	0.007	Significant
Error	12	1577.8	131.5	–	–	
Total	17	14,400.0				

Table 8 ANOVA for average surface roughness parameter

Source	DF	Adj. SS	Adj. MS	*F*	*P*	Remark
Cutting tool	1	5.3029	5.3029	8.70	0.012	Significant
Cutting speed	2	4.8058	2.4029	3.94	0.048	Significant
Feed rate	2	0.4801	0.2401	0.39	0.683	Not significant
Error	12	7.3148	0.6096	–	–	
Total	17	17.9037				

speed, followed by the feed rate and lastly from the selection of the cutting tool. In a similar fashion, the *F* statistics provides the same message; the relative importance of the cutting speed is higher, afterward the feed rate. Based on the *P* value, it can be asserted that the cutting speed and feed rate both are statistically significant factors.

Next, Table 7 lists the ANOVA for feed force. Here, one can see that like main cutting force, the highest variation is contributed by the cutting speed, and then the feed rate followed by the tool insert. However, all the factors are found statistically significant based on the *P* value (<0.05). The *F* value demonstrates that the cutting speed has a far more important role compared to the other two factors. In this respect, it is understood that by controlling the cutting speed, the feed force can be controlled and favorably turned to better machinability.

On the other side, Table 8 shows the ANOVA for the average surface roughness parameter. Herein, it is discernable that tool configuration causes the highest variation in surface roughness. The second next variation is created by the cutting speed, which is somewhat close to the variation of the cutting speed. Compared to these, the deviation instigated by the feed rate is trivial. The *F* statistics also reveals the same outcome. Based on the *P* value, it is appreciable that the tool insert configuration and cutting speed are statistically significant. One must notice here that a higher coefficient of variation of surface roughness, described in Section 3.1, is accredited to the wider variation of surface roughness caused by the tool insert configuration and cutting speed.

Figure 5 shows the percentage contribution (PC) of factors on the responses. PC is calculated by obtaining the ratio of SS with respect to total SS (from ANOVA tables). Herein, quantitative values depict that the cutting speed exerted ~71% contribution (highest) on the cutting forces while 26.84% on surface roughness. Furthermore, the influence of the feed rate on forces (~14%) and effect of tool insert configuration on surface roughness (~29.6%) are notable.

Table 7 ANOVA for feed force

Source	DF	Adj. SS	Adj. MS	*F*	*P*	Remark
Cutting tool	1	272.2	272.2	5.03	0.045	Significant
Cutting speed	2	4272.3	2136.17	39.49	0.000	Significant
Feed rate	2	816.3	408.17	7.55	0.008	Significant
Error	12	649.1	54.09	–	–	
Total	17	6010.0				

3.3 Main effects and 3D response surface plots

The movement of the mean of responses (for instance, the mean of main cutting force) with respect to the investigated input parameters is studied herein. One can see that Fig. 6 illustrates the main effects plot of main cutting force with respect to the tool insert, cutting speed, and feed rate. It is appreciable that use of the SNMM insert is associated with lower main cutting force, so are using the lowest cutting speed and highest feed rate. Further noticeable is the change in cutting speed over its range, which causes a great range of cutting force, significantly greater than the range caused by the other factors. This is aligning with the results caused by the ANOVA. Figure 7 shows the main effects plot for the feed force. Like P_z, the feed force presents a similar trend except that the SNMG tool insert divulged a lower feed force. Therefore, the lowest feed force is found at the lowest cutting speed, highest feed rate, and in machining under the SNMG tool insert. Figure 8 depicts the main effects plot for average surface roughness. Unlike the previous two responses, herein, the tool insert plays a dominant role in defining surface roughness. The SNMM insert produced the lowest surface roughness (more than 50% reduced mean R_a compared to that of the SNMG insert). Then, the behavior of the cutting speed is different too. The lowest mean surface roughness is achievable at a cutting speed of 112 m/min and at a feed rate of 0.12 mm/rev (lowest).

The 3D response surface plot is an effective graphical tool that enables to visualize the behavior of a response with respect to two variables at a time [33], in this case with respect to the cutting speed and feed rate. Figure 9 exhibits the 3D surface plots of the investigated responses, i.e., (a) main cutting force, (b) feed force, and (c) average surface roughness. First of all, it is appreciable that the relations which are depicted in these figures are very complex, consisting of several peaks and crests. In continuation, both the cutting forces signify almost similar trends wherein a lower feed rate and higher cutting speed tend to generate higher cutting forces and a higher feed rate and lower cutting speed are responsible for

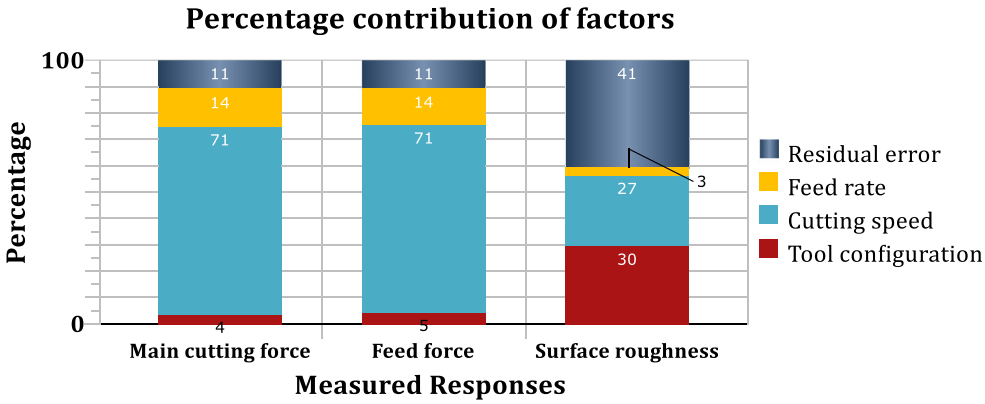

Fig. 5 Percentage contribution of the factors on the responses

lower cutting forces. In the case of surface roughness, different scenarios prevail. Herein, the feed rate has little influence, and a cutting speed of 112 m/min is associated with the lowest surface roughness (understandable from the crest existing at V_c = 112 m/min). Note that a higher cutting speed is reflected with higher surface roughness.

3.4 Residual analysis of responses

Residual plots are critical tools for evaluating the goodness of fit of the models [31]. There are four plots: the normal probability plot, then the residual versus fitted plot, histogram of the residuals, and the residual versus observation order plot. Figure 10 shows the residual plot for main cutting force. Here, in the normal probability plot, the data points are reasonably close to the straight line; thereby, the assumption for normality remains valid [34]. The residual versus fitted plots show that data points are randomly scattered; therefore, the assumption for constant variance is correct [34]. Nevertheless, some skewness in the left side is noticeable from the histogram plot. Finally, in the residual versus order plot, an increasing trend is visible in the first segment and after that, ups and downs are appreciable. This can be due to the contribution of SNMM and SNMG tool-induced cutting force.

Figure 11 illustrates the residual plots for feed force. The residuals are normally distributed; constant variance is valid; however, little skewness in the left tail and increasing and decreasing correlations are visible in the initial and later stages. Figure 12 shows the residual plot for surface roughness. Herein, residuals are normally distributed, three groups of data are visible, skewness is not visible, and increasing and decreasing patterns are noticeable.

3.5 Effects of cutting speed and feed on surface roughness

Figure 13 exhibits the behavior of the average surface roughness parameter with the progression of the cutting speed at different feed rates operated by using the SNMG and SNMM tool inserts. When machined by the SNMM insert, surface roughness gradually increases with the cutting speed, and this increment is higher at higher speeds. This can be attributed to the expedited tool wear originated at increased cutting speed which makes the tools blunt [35]. While machining by the SNMG insert, the pattern of surface roughness is almost reciprocal, i.e., reduces with an increasing cutting speed. In this case, the effect of reduced friction due to a higher cutting speed and less chattering associated with no-BUE formation on the tool contributed to this lowering of surface roughness [5, 33].

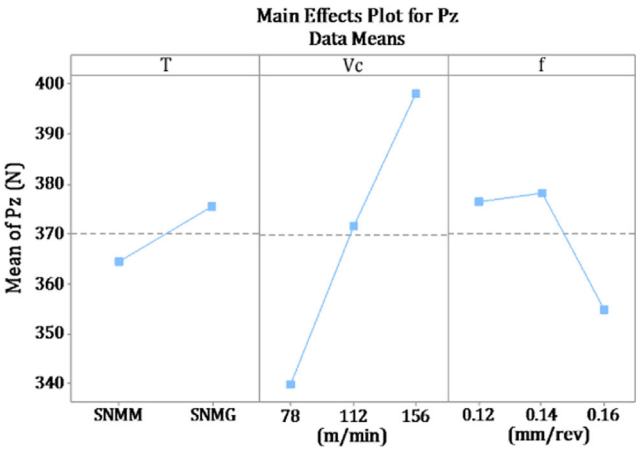

Fig. 6 Main effects plot for main cutting force

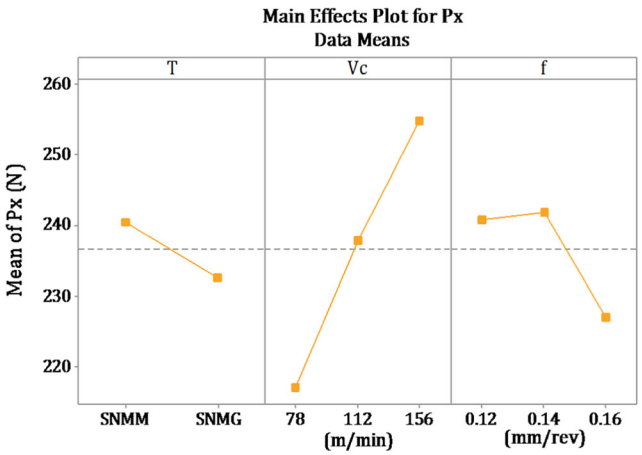

Fig. 7 Main effects plot for feed force

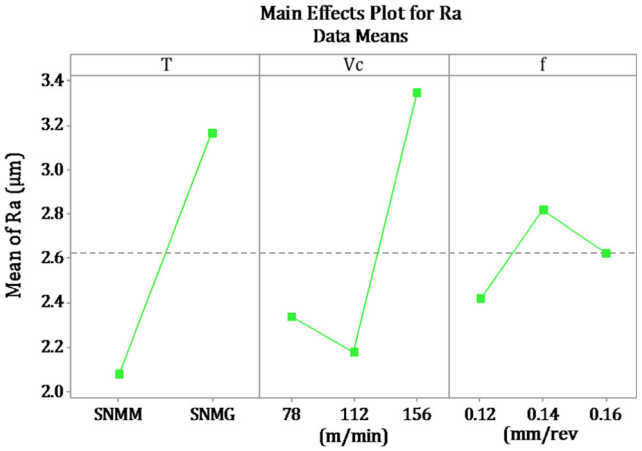

Fig. 8 Main effects plot for average surface roughness parameter

Noticeably, at a higher speed, this increment is very trivial. On the other side, the effect of another cutting parameter, i.e., the feed rate, is not coherent; however, in the SNMG insert, the lowest feed rate induced the lowest surface roughness whereas in the case of the SNMM insert, the highest feed rate produced the lowest surface roughness. Presumably, the results found for the SNMG insert are in good agreement with the theoretical relation of surface roughness and feed rate, i.e., surface roughness is proportional to the square of the feed rate for a constant tool nose radius [5]; nonetheless, the behavior of surface roughness for the SNMM insert shows, unexpectedly, the opposite of the theoretical relation. The prime reason for this opposing behavior may be the proportionate increment in the tool nose radius with the augmented feed rate under the application of cryogenic cooling, which also contributed to the material's instantaneous thermal treatment and hardening [36]. This hardening of the material induces better finishing by generating lower surface roughness.

3.6 Effects of cutting speed and feed on cutting forces

Figure 14a shows a steady increase in main cutting force with increasing cutting speed; besides, the highest feed rate for both inserts creates the lowest cutting force. The former point is explained by the fact that the increased cutting speed imparts higher material straining for chip formation which in turn engendered elevated cutting zone temperature [30, 36]. Presumably, the application of cryogenic cooling reduces the cutting zone temperature [8], yet as a side effect, it created material hardening and thereby an augmented cutting force was required at an accelerated cutting speed. Furthermore, as mentioned earlier, the rapid tool wear at higher cutting speed hinders the performance of the tool insert and the tool becomes blunt. To compensate for this loss, while machining at a higher cutting speed, a higher cutting force is required for chip shearing. Furthermore, the change in chip formation along with increased friction tends to accumulate machining forces [10].

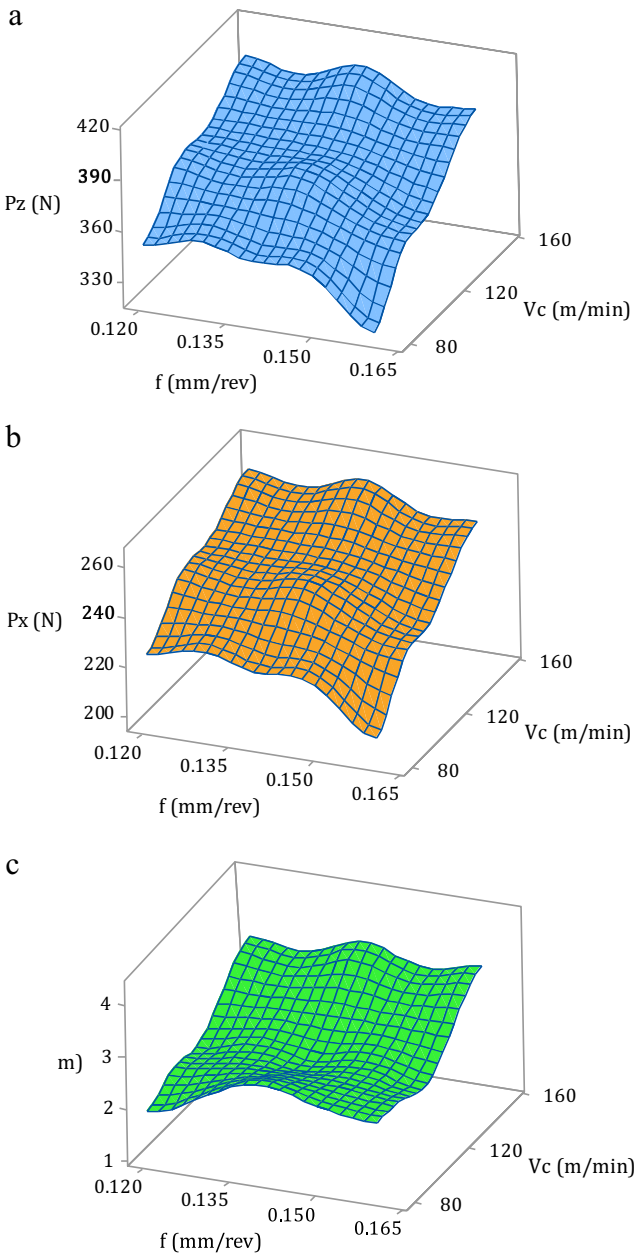

Fig. 9 3D surface plots of **a** main cutting force, **b** feed force, and **c** average surface roughness with respect to cutting speed and feed rate

Figure 14b reveals a similar trend for feed force wherein the SNMG insert is associated with lower feed force generation. Similar causes can be attributed to this feed force pattern.

3.7 Predictive model by ANN

After using the randomly preselected training data in ANN model construction, the network structure was determined with an optimized error value right after the halting of generalization. Figure 15 shows the designed networks with specified hidden neurons for main cutting force, feed force, and surface roughness under the application of liquid nitrogen.

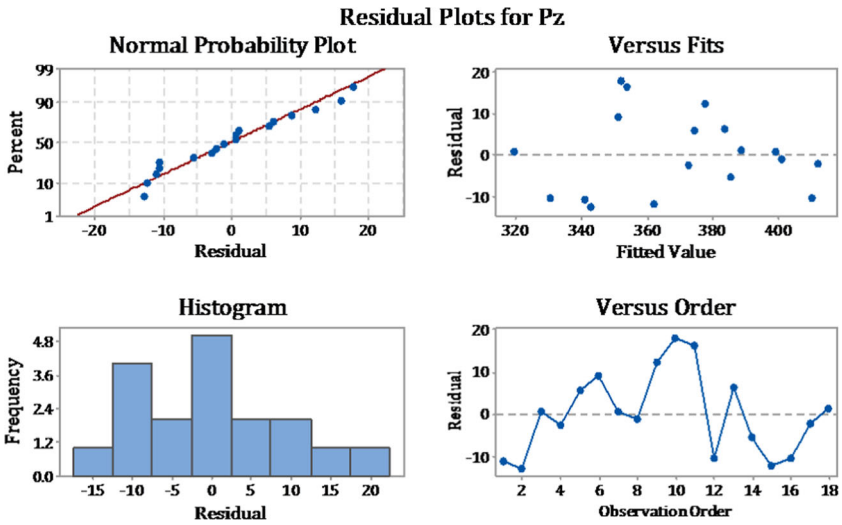

Fig. 10 Residual plots for main cutting force

Here, w and b are the assigned weights and biases for the neurons, respectively. According to Fig. 15, the value of main cutting force (P_z) has been predicted by using the 3-20-1 structure and feed force (P_x) by using the 3-15-1 structure. During the trial-and-error stage of determining the hidden neuron numbers for surface roughness, 2 × no. of input neurons + 1 = 7, suggested by Lippmann [37], has been implemented and provided the best result. Thus, the 3-7-1 structure has been used for surface roughness (R_a) prediction corresponding to the input parameter setting. However, there is no certainty that this hidden node number works accurately in other application areas. In addition, these constructed models need to be tested to ascertain the level of prediction accuracy for the data outside of the training data which is done under Section 3.9.

3.8 Quadratic model by RSM

The full quadratic models (equations) of main cutting force, feed force, and surface roughness have been developed by using the RSM for the two different inserts, i.e., SNMG and SNMM, and are shown by Eqs. 6–11, respectively. The corresponding correlation coefficient (R^2) has also been mentioned. Bouacha et al. [38], when they developed response surface models of forces and surface roughness, also found almost similar values of R^2. Therefore, these R^2 values suggest that the formulated RSM models can be used for the prediction of cutting forces (main and feed) and surface roughness [16].

$$\text{SNMG}\quad P_z = -241 - 1.106\,V_c + 10,170\,f - 0.0004\,{V_c}^2 - 44,409\,f^2 + 12.86\,V_c \times f \left(R^2 = 98.54\%\right) \tag{6}$$

$$\text{SNMM}\quad P_z = -408 - 0.562\,V_c + 10,893\,f - 4 \times 10^{-4}\,{V_c}^2 - 44,409\,f^2 + 12.86\,V_c \times f \left(R^2 = 98.54\%\right) \tag{7}$$

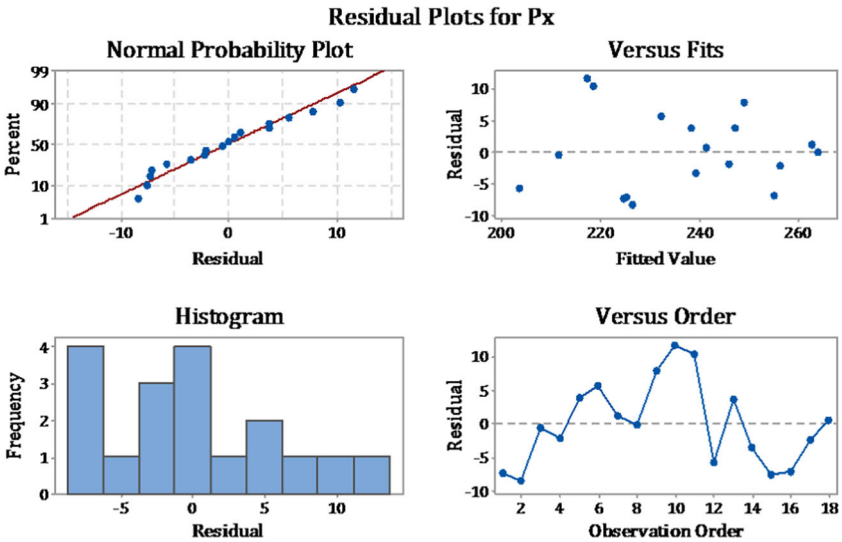

Fig. 11 Residual plots for feed force

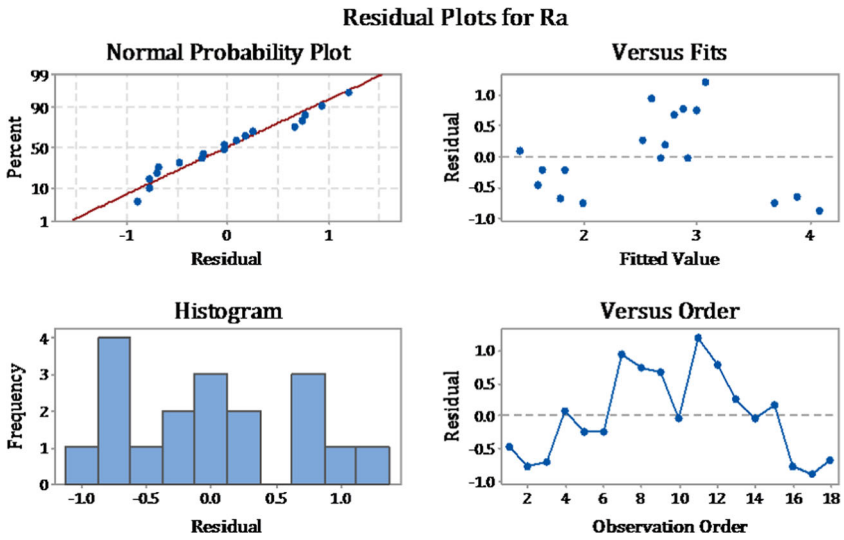

Fig. 12 Residual plots for average surface roughness

$$\text{SNMG}\quad P_x = -136 + 0.961\,V_c + 4937\,f - 0.00205\,{V_c}^2 - 19,440\,f^2 - 1.08\,V_c \times f \left(R^2 = 96.54\%\right) \tag{8}$$

$$\text{SNMM}\quad P_x = -230 + 1.202\,V_c + 5459\,f - 0.00205\,{V_c}^2 - 19,440\,f^2 - 1.08\,V_c \times f \left(R^2 = 96.54\%\right) \tag{9}$$

$$\text{SNMG}\quad R_a = -13.6 - 0.1085\,V_c + 309\,f + 5.55 \times 10^{-4}\,{V_c}^2 - 944\,f^2 - 0.199\,V_c \times f \left(R^2 = 97.21\%\right) \tag{10}$$

$$\text{SNMM}\quad R_a = -16.1 - 0.0708\,V_c + 288\,f + 5.55 \times 10^{-4}\,{V_c}^2 - 944\,f^2 - 0.199\,V_c \times f \left(R^2 = 97.21\%\right) \tag{11}$$

3.9 Comparison of ANN and RSM models

The mean absolute percentage error (MAPE) for the ANN and RSM models has been computed for main cutting force, feed force, and surface roughness after calculating the absolute percentage error (APE) for each experimental and predicted response. These values are listed in Table 9. It is discernable from Table 9 that the MAPE for main cutting force, feed force, and surface roughness is 2.93, 2.32, and 12.36%, respectively, for the predicted response values by ANN whereas 1.73, 1.63, and 9.06%, respectively, for the RSM predicted response values. Although the average errors of main cutting force and feed force are comparatively low, the errors of surface roughness for both ANN and RSM models are high. This high prediction error is attributable to the undefined randomness of surface roughness, which has resulted from the contribution of the feed rate and generated cutting temperature due to friction and non-uniform hardness distribution within the material [32]. However, the response surface method showed an accuracy that is higher than the accuracy of the neural network-based models. However, a comparative study of the RSM and ANN conducted by Sahoo et al. [39] found superior performance of the ANN. The RSM-based surface roughness prediction model even though suggests a MAPE of 9%, which is greater than the average prediction error level derived by Azam et al. [40] for high-strength low-alloy steel by using the RSM, yet the developed model is acceptable as the error rate lay below 10% and the error rate found by Basheer et al. [41] for a metal matrix composite.

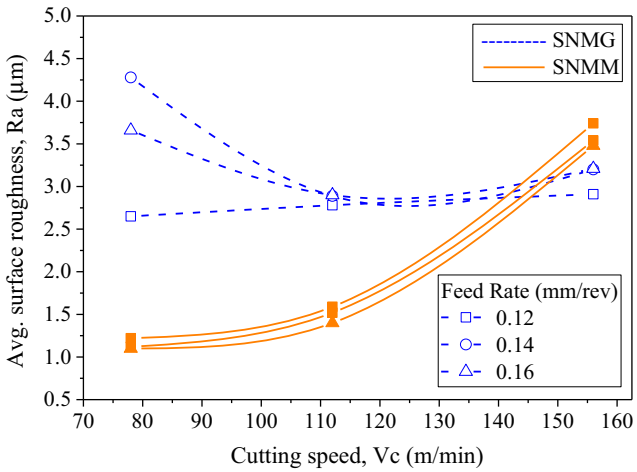

Fig. 13 Effect of cutting speed and feed rate on average surface roughness

The formulated models were put into the testing phase to evaluate prediction capability for a parameter setting that is different from the training data set [33]. The results of the model testing are shown in Fig. 16, wherein the *y*-axis represents the response and the *x*-axis shows the testing run

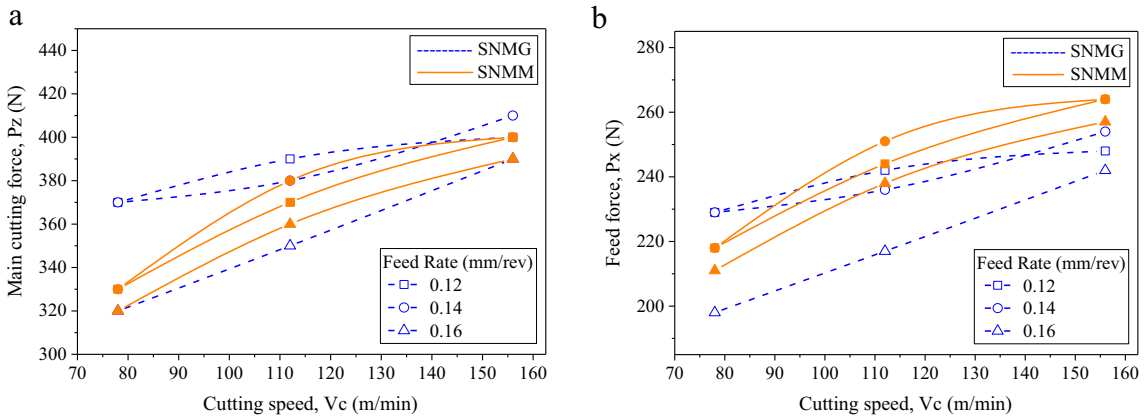

Fig. 14 Effect of cutting speed and feed rate on **a** cutting force and **b** feed force

orders (italicized data, as in the sequence in Table 9). Here, it is noticeable that the response surface model, for most of the runs, generated response values closer to the actual response values. In the case of main cutting force, the RSM and ANN models showed a mixed tendency of over- and underestimation. For the feed force, the ANN exhibited overestimation and the RSM showed mixed estimation. Lastly, for surface roughness, the ANN revealed overestimation for all runs except the first run and the RSM provided a combination of over- and underestimation. In sum, on the ground of testing of non-trained data, the response surface-based models are more accurate in prediction. This superior accuracy of the RSM was established due to the fact that the quadratic relation of response and factors defined by the RSM agreed completely for these cases [32].

The regression plots of the actual and predicted forces and surface roughness are illustrated in Fig. 17. These figures are constructed for the total data sets (training and testing). The *y*-axis shows the predicted value while the *x*-axis represents the actual values of the response. The dot line is the ideal straight line which indicates an equal relation between the actual and predicted responses, whereas the solid line represents the regression line showing the best fit between the predicted and actual responses. The dot points represent the actual versus predicted response plot.

Figure 17a shows that the ANN model has a comparatively low value of correlation coefficient (91.51%) as the points are

Fig. 15 ANN prediction models

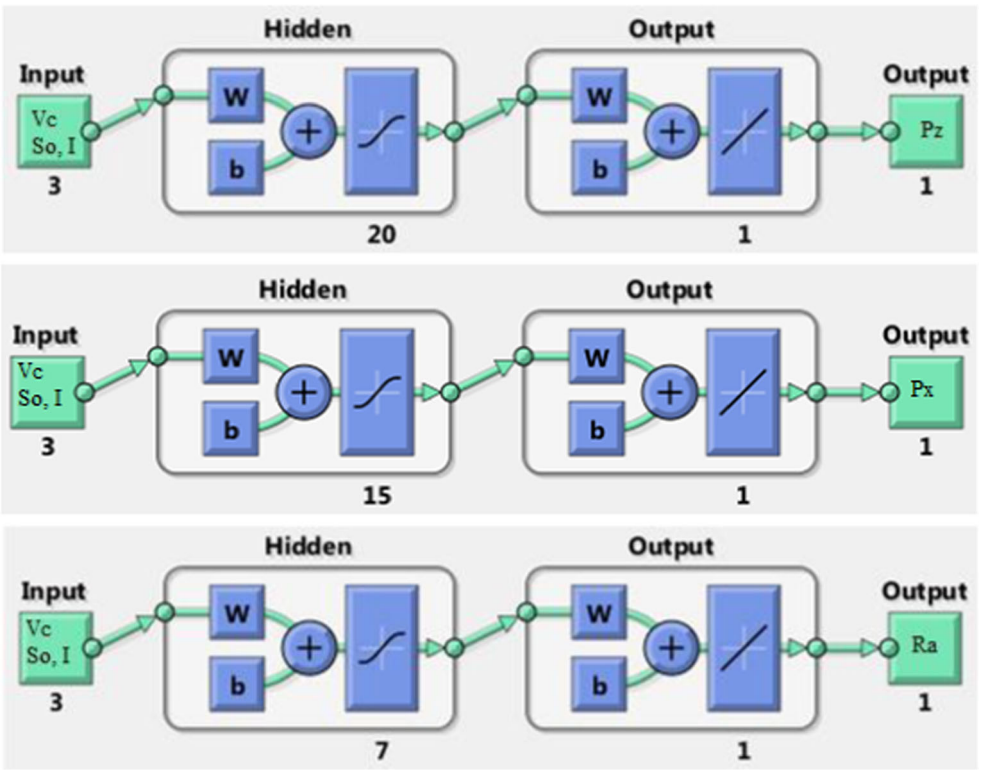

Table 9 Absolute percentage error of ANN and RSM models

SL no.	Artificial neural network			Response surface method		
	APE-P_z	APE-P_x	APE-R_a	APE-P_z	APE-P_x	APE-R_a
1	2.4806	0.5922	19.8207	0.4140	0.0209	11.9022
2	6.5098	2.7790	3.5468	1.0161	0.5283	22.3878
3	5.0450	2.2289	26.3636	1.6059	1.7751	8.1249
4	*3.6726*	0.7813	6.2367	*3.1356*	2.4150	15.514
5	6.8666	*9.8095*	*14.9616*	0.3302	*3.7203*	*13.214*
6	*4.0475*	*2.2249*	3.6604	*2.5580*	*1.4832*	8.5277
7	*2.0394*	1.7817	*18.5061*	*1.5809*	0.8385	*26.273*
8	0.7262	*1.0017*	*30.0652*	1.5878	*1.5975*	*18.632*
9	1.9640	1.6752	*15.2863*	1.3426	1.3903	*0.3076*
10	4.4365	3.4011	15.8095	0.0366	2.0767	3.2485
11	3.7117	4.3740	16.0331	0.2406	0.9130	1.9766
12	1.7685	0.1465	22.9432	0.0193	0.8734	7.7836
13	2.1532	*4.2291*	8.8101	0.4003	*3.4338*	4.8638
14	0.0635	1.5253	2.6294	0.6478	0.3142	2.1715
15	2.5363	0.3624	*0.5471*	0.2387	1.2513	*7.0390*
16	*2.3747*	0.7248	9.7681	*7.4099*	1.4811	2.8562
17	0.0907	*3.8302*	1.8346	0.5047	*5.1339*	3.6309
18	*2.2859*	0.3893	5.6690	*7.9899*	0.0380	4.5605
MAPE	2.9318	2.3254	12.3606	1.7255	1.6269	9.0566

Italicized numbers indicate APE for testing data

scattered, while the RSM model possesses a correlation coefficient value (94.85%) that is higher than that of the ANN model due to the existing closeness among the points. Similarly, Fig. 17b shows that the ANN regression curve shifted to the left side at the region of lower feed force; however, at higher feed force, the ideal and fit curves inclined closely to each other. The RSM regression fitting is found to be in good accordance (96.38%) with the ideal actual-predicted response as the experimental values of the forces are closely aligned. Figure 17c reveals quite alarming results when predicted by the ANN model as the experimental values formed clustered into two groups—one at the higher values of surface roughness and the other at the low values of surface roughness. In addition, the variability of the data is very high and results in a lower value of the correlation coefficient (91.03%) than that of the RSM (96.69%). Though, in the RSM model, there exist two groups of data at the lower and higher ranges, the variability of the data is uniformly distributed against the ideal curve and hence reveals a better value of the correlation coefficient.

Even though the accuracy of the ANN model is expected to be higher for a good number of training data, the limitation of the resource [15] (machine, material, time, etc.) has forced us to conduct this experiment with 18 experimental trials. This fact might be a possible reason for the ANN model to exhibit the higher error values for the training data. Trade-off between

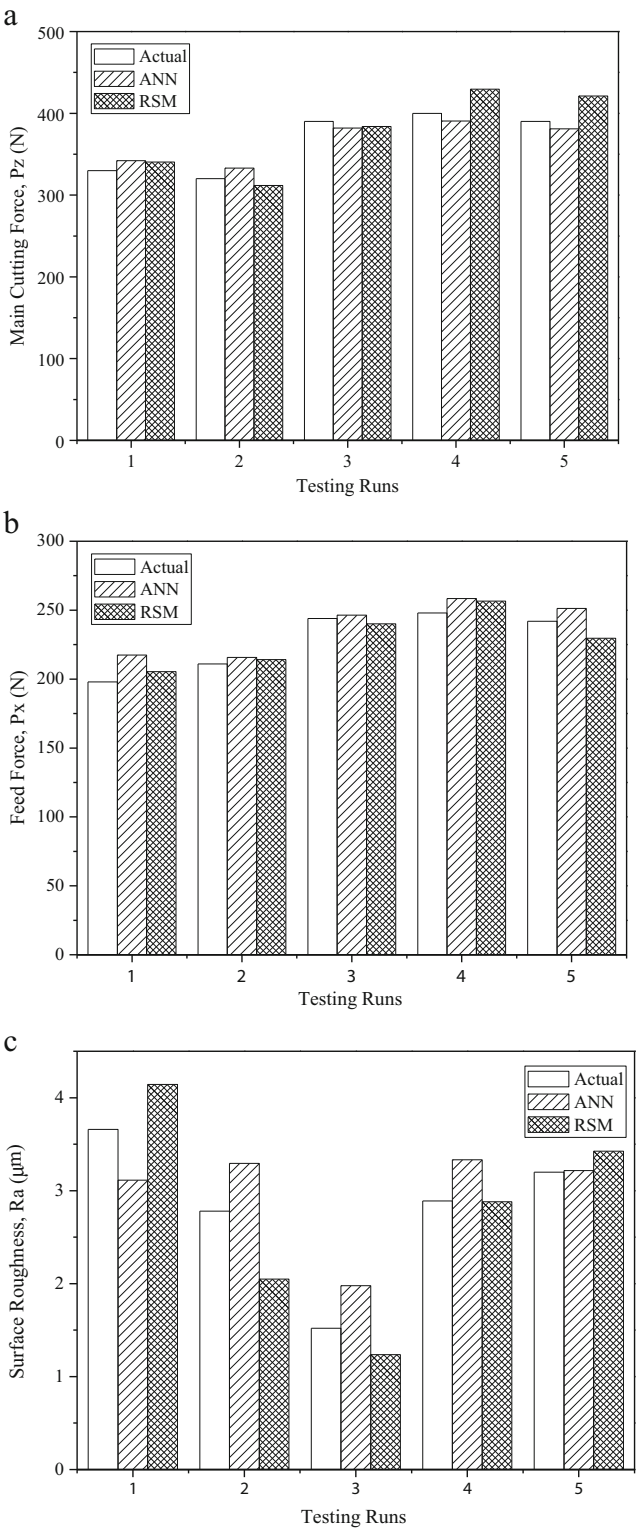

Fig. 16 Testing of ANN and RSM models for **a** main cutting force, **b** feed force, and **c** average surface roughness

cost-time and accuracy is thus required. After a lot of trial-and-error iterations to determine the number of hidden neurons, the best results providing network structures are determined in this work to predict the machining responses. These network

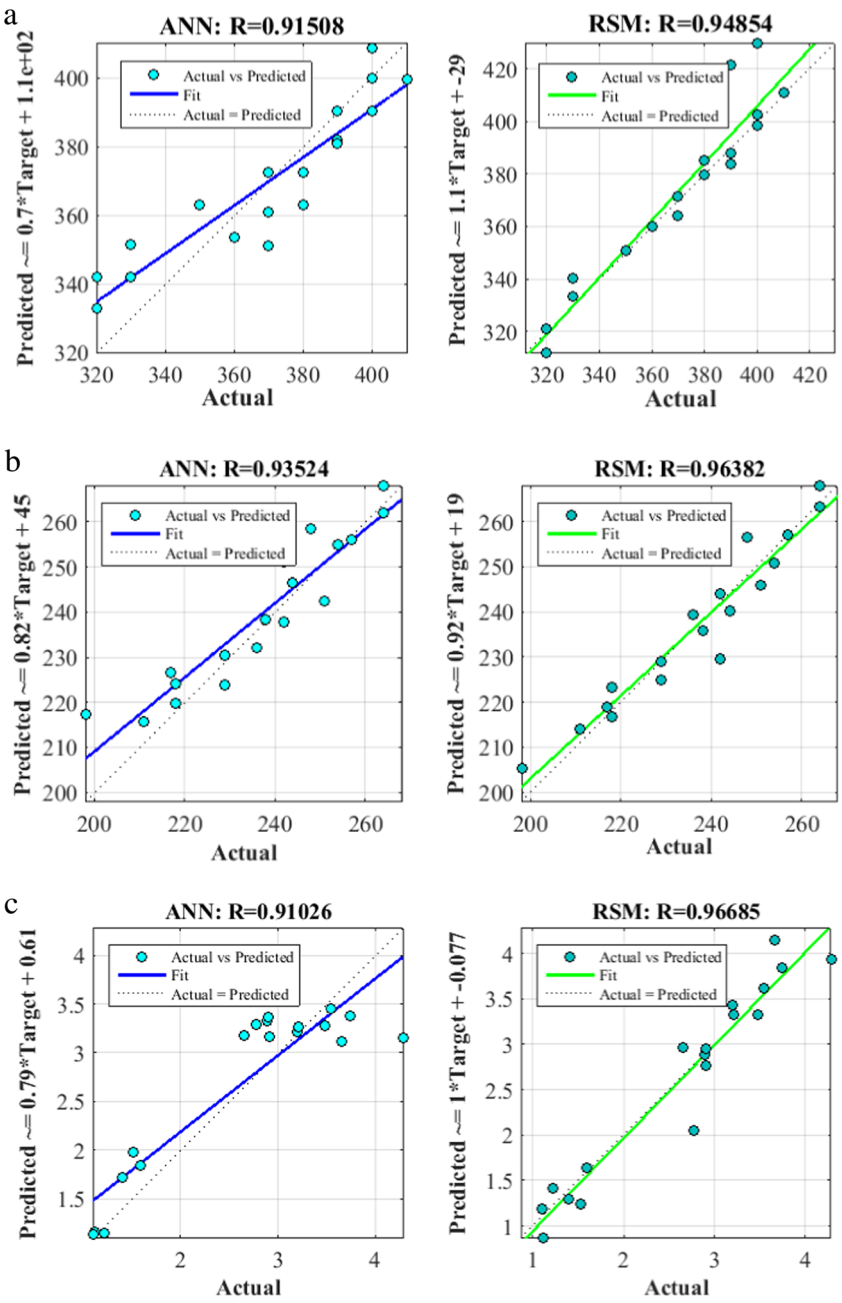

Fig. 17 Regression plots of predicted and actual responses for **a** main cutting force, **b** feed force, and **c** average surface roughness

structures are 3-20-1, 3-15-1, and 3-7-1 (trained by Bayesian regularization) for main cutting force, feed force, and surface roughness, respectively.

Table 10 Parameters for optimization of multiple characteristics

Response	Goal	Lower	Target	Upper	Weight	Importance
R_a	Minimize	1.1	1.1	4.28	1	1
P_x	Minimize	198	198	264.0	1	1
P_z	Minimize	320	320	410.0	1	1

3.10 Optimization by desirability function

In this section, the minimization of main cutting force, feed force, and surface roughness is performed by using the desirability function. Since multiple responses are involved, herein, the optimization has turned to be a composite desirability-based optimization [42]. The optimization has been conducted within some constraints and objectives, which are listed in Table 10. The weights and importance for all the responses are given as 1.0, that is, all the responses are equal in all perspectives. With a view to attain these objectives, the optimization has been conducted, which is displayed in Fig. 18.

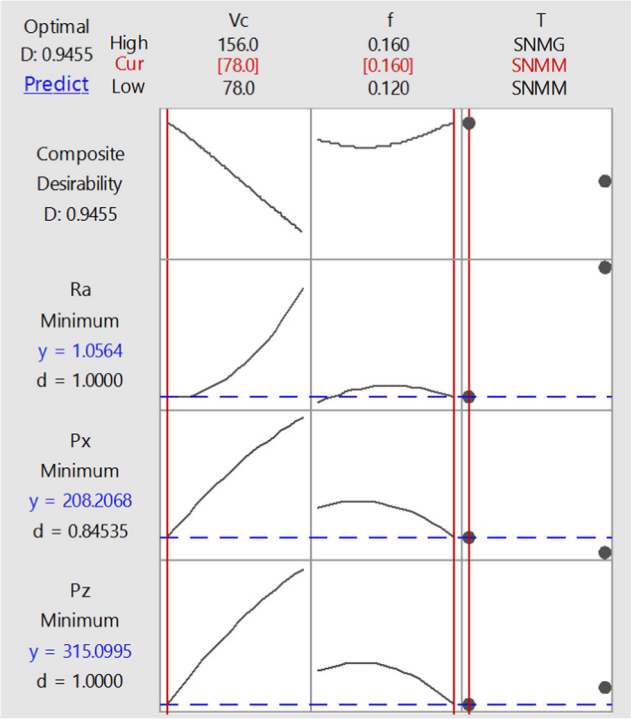

Fig. 18 Optimization of multiple responses by composite desirability function

The results of the optimization provided by the composite desirability function and its comparison with that of the experimental value are shown in Table 11. One can see that the composite desirability is 0.9455, which makes the optimum results acceptable. The optimum parameter values are a cutting speed of 78 m/min, a feed rate of 0.16 mm/rev, and use of the SNMM cutting tool insert. Consequently, by using these cutting parameter values, it is possible to simultaneously achieve a surface roughness of 1.05 μm, main cutting force of 315.1 N, and feed force of 208.21 N. One can further notice that the actual experimental results, which are the values of surface roughness, main cutting force, and feed force, are very close to the optimum outcomes derived by the composite desirability function. To be specific, the percentage changes between the theoretical optimum and experimental optimum results are 4.55, 1.32, and 1.53% for surface roughness, main cutting force, and feed force, respectively. These deviations are small and thereby declare the optimum results of this study as acceptable. Similar deviations can be found in the work reported by Mia et al. [21].

4 Conclusions

In this work, an attempt has been made to investigate the effects of machining parameters during turning of difficult-to-cut Ti-6Al-4V alloy. Furthermore, two predictive models of main cutting force, feed force, and surface roughness were developed by using the RSM and ANN. The optimization of these responses was also performed by using the composite desirability function. The experimental data were collected under the application of environmentally benign cryogenic machining condition. The cutting speed, feed rate, and tool insert configurations were considered as the influential factors in this study. From the experimental runs, subsequent model development, and result analysis, the following concluding notes can be extracted:

- The SNMM insert is found to provide lower surface roughness when subjected to low-cutting-speed machining. However, a low cutting speed is counter-productive; thereby, it is suggested to maintain the cutting speed not more than 110 m/min. Herein, the effect of the feed rate is recognized as insignificant.
- A lower-to-medium cutting speed is deemed favorable as a balance between low cutting force and feed force with productivity. Unexpectedly, the highest feed rate produced the lowest forces, which yet maintain good agreement with the lowering of surface roughness. In this case, the recommended cutting speed is ~110 m/min and feed rate 0.16 mm/rev.
- The RSM models of forces and surface roughness revealed better accuracy with untrained data compared to the ANN models.
- The mathematical models (by the RSM) showed very promising values of correlation coefficient (above 96%) and thus reflect the appropriate relation of the dependent and independent variables; thus, these equations are recommended as usable for predicting surface roughness and cutting forces in turning Ti-6Al-4V alloy under liquid nitrogen-assisted cryogenic condition.
- Optimum results are as follows: average surface roughness of 1.05 μm, feed force of 208 N, and main cutting force of 315 N, attainable by using a coated WC insert of SNMM 120408 configuration at a cutting speed of 78 m/min, a feed rate of 0.16 mm/rev, and a depth of cut of 1.0 mm under cryogenic LN_2 condition.

Table 11 Comparison of the optimum results by composite desirability function with actual experimental results

Run	V_c (m/min)	f (mm/rev)	T	R_a (μm)	P_x (N)	P_z (N)	Composite desirability
Desirability optimization	78	0.16	SNMM	1.05	208.21	315.1	0.9455
Actual run	78	0.16	SNMM	1.10	211	320	–
% Deviation with respect to actual run				4.55	1.32	1.53	–

- In this study, the inclusion of a textual variable such as tool insert configuration has been possible by using an artificial neural network and hence widens the capability to modeling the machining performance characteristics more effectively and in extended areas of machining industries.

Acknowledgements The authors are grateful to the Directorate of Advisory, Extension and Research Services (DAERS), BUET, Dhaka, Bangladesh, for providing research fund, Sanction No. DAERS/CASR/R-01/2015/DR-2181 (71), and to the Department of Industrial and Production Engineering, BUET, Bangladesh, for allowing us to use the laboratory facility for experimental purposes.

References

1. Su Y, He N, Li L, Li X (2006) An experimental investigation of effects of cooling/lubrication conditions on tool wear in high-speed end milling of Ti-6Al-4V. Wear 261(7):760–766
2. Hong H, Riga A, Gahoon J, Scott C (1993) Machinability of steels and titanium alloys under lubrication. Wear 162:34–39
3. Rahman M, Wong YS, Zareena AR (2003) Machinability of titanium alloys. JSME International Journal Series C 46(1):107–115
4. Paul S, Dhar N, Chattopadhyay A (2001) Beneficial effects of cryogenic cooling over dry and wet machining on tool wear and surface finish in turning AISI 1060 steel. J Mater Process Technol 116(1):44–48
5. Mia M, Dhar NR (2016) Optimization of surface roughness and cutting temperature in high-pressure coolant-assisted hard turning using Taguchi method. The International Journal of Advanced Manufacturing Technology:1–15. doi:10.1007/s00170-016-8810-2
6. Bashir MA, Mia M, Dhar NR (2016) Investigations on surface milling of hardened AISI 4140 steel with pulse jet MQL applicator. Journal of The Institution of Engineers (India): Series C:1–14. doi:10.1007/s40032-016-0277-2
7. Islam AK, Mia M, Dhar NR (2016) Effects of internal cooling by cryogenic on the machinability of hardened steel. The International Journal of Advanced Manufacturing Technology:1–10. doi:10.1007/s00170-016-9373-y
8. Ghosh S, Rao PV (2015) Application of sustainable techniques in metal cutting for enhanced machinability: a review. J Clean Prod 100:17–34
9. Machai C, Biermann D (2011) Machining of β-titanium-alloy Ti–10V–2Fe–3Al under cryogenic conditions: cooling with carbon dioxide snow. J Mater Process Technol 211(6):1175–1183
10. Sun S, Brandt M, Palanisamy S, Dargusch MS (2015) Effect of cryogenic compressed air on the evolution of cutting force and tool wear during machining of Ti–6Al–4V alloy. J Mater Process Technol 221:243–254
11. Vazquez E, Gomar J, Ciurana J, Rodríguez CA (2015) Analyzing effects of cooling and lubrication conditions in micromilling of Ti6Al4V. J Clean Prod 87:906–913
12. Moura RR, da Silva MB, Machado ÁR, Sales WF (2015) The effect of application of cutting fluid with solid lubricant in suspension during cutting of Ti-6Al-4V alloy. Wear 332:762–771
13. da Silva RB, Machado ÁR, Ezugwu EO, Bonney J, Sales WF (2013) Tool life and wear mechanisms in high speed machining of Ti–6Al–4V alloy with PCD tools under various coolant pressures. J Mater Process Technol 213(8):1459–1464
14. Xie J, Luo M, Wu K, Yang L, Li D (2013) Experimental study on cutting temperature and cutting force in dry turning of titanium alloy using a non-coated micro-grooved tool. Int J Mach Tools Manuf 73:25–36
15. Zain AM, Haron H, Sharif S (2010) Prediction of surface roughness in the end milling machining using artificial neural network. Expert Syst Appl 37(2):1755–1768
16. Hasçalık A, Çaydaş U (2008) Optimization of turning parameters for surface roughness and tool life based on the Taguchi method. Int J Adv Manuf Technol 38(9–10):896–903
17. Hashmi KH, Zakria G, Raza MB, Khalil S (2015) Optimization of process parameters for high speed machining of Ti-6Al-4V using response surface methodology. The International Journal of Advanced Manufacturing Technology:1–10
18. Moufki A, Dudzinski D, Le Coz G (2015) Prediction of cutting forces from an analytical model of oblique cutting, application to peripheral milling of Ti-6Al-4V alloy. Int J Adv Manuf Technol 81(1–4):615–626
19. Ramesh S, Karunamoorthy L, Palanikumar K (2012) Measurement and analysis of surface roughness in turning of aerospace titanium alloy (gr5). Measurement 45(5):1266–1276
20. Mia M, Khan MA, Dhar NR (2016) Performance prediction of high-pressure coolant assisted turning of Ti-6Al-4V. The International Journal of Advanced Manufacturing Technology:1–13. doi:10.1007/s00170-016-9468-5
21. Mia M, Khan MA, Rahman SS, Dhar NR (2016) Mono-objective and multi-objective optimization of performance parameters in high pressure coolant assisted turning of Ti-6Al-4V. The International Journal of Advanced Manufacturing Technology:1–10. doi:10.1007/s00170-016-9372-z
22. Dhar N, Kamruzzaman M (2007) Cutting temperature, tool wear, surface roughness and dimensional deviation in turning AISI-4037 steel under cryogenic condition. Int J Mach Tools Manuf 47(5):754–759
23. Khan MA, Mia M, Dhar NR (2016) High-pressure coolant on flank and rake surfaces of tool in turning of Ti-6Al-4V: investigations on forces, temperature, and chips. The International Journal of Advanced Manufacturing Technology:1–15. doi:10.1007/s00170-016-9511-6
24. Mia M, Khan MA, Dhar NR (2016) High-pressure coolant on flank and rake surfaces of tool in turning of Ti-6Al-4V: investigations on surface roughness and tool wear. The International Journal of Advanced Manufacturing Technology:1–10. doi:10.1007/s00170-016-9512-5
25. Hanafi I, Khamlichi A, Cabrera FM, Nuñez López PJ (2012) Prediction of surface roughness in turning of PEEK cf30 by using an artificial neural network. Journal of the Chinese Institute of Industrial Engineers 29(5):337–347
26. MacKay DJ (1992) Bayesian interpolation. Neural Comput 4(3):415–447
27. Foresee FD, Hagan MT Gauss-Newton approximation to Bayesian learning. In: International conference on neural networks, 1997. 1997. IEEE, pp 1930–1935
28. Ezugwu E, Fadare D, Bonney J, Da Silva R, Sales W (2005) Modelling the correlation between cutting and process parameters in high-speed machining of Inconel 718 alloy using an artificial neural network. Int J Mach Tools Manuf 45(12):1375–1385
29. Draper NR, Smith H, Pownell E (1966) Applied regression analysis, vol 3. Wiley, New York
30. Mia M, Bashir MA, Khan MA, Dhar NR (2016) Optimization of MQL flow rate for minimum cutting force and surface roughness in end milling of hardened steel (HRC 40). The International Journal of Advanced Manufacturing Technology:1–16. doi:10.1007/s00170-016-9080-8
31. Mia M, Razi MH, Ahmad I, Mostafa R, Rahman SMS, Ahmed DH, Dey PR, Dhar NR (2017) Effect of time-controlled MQL pulsing on surface roughness in hard turning by statistical analysis and artificial neural network. The International Journal of Advanced Manufacturing Technology:1–13. doi:10.1007/s00170-016-9978-1

32. Mia M, Dhar NR (2016) Response surface and neural network based predictive models of cutting temperature in hard turning. J Adv Res 7(6):1035–1044
33. Mia M, Dhar NR (2016) Prediction of surface roughness in hard turning under high pressure coolant using artificial neural network. Measurement 92:464–474
34. Mia M, Al Bashir M, Dhar NR Effects of cutting parameters and machining environments on surface roughness in hard turning using design of experiment. In: AIP conference proceedings, 1754
35. Ayed Y, Germain G, Ammar A, Furet B (2015) Tool wear analysis and improvement of cutting conditions using the high-pressure water-jet assistance when machining the Ti17 titanium alloy. Precis Eng 42:294–301
36. Dinesh S, Senthilkumar V, Asokan P, Arulkirubakaran D (2015) Effect of cryogenic cooling on machinability and surface quality of bio-degradable ZK60 Mg alloy. Mater Des 87:1030–1036
37. Lippmann R (1987) An introduction to computing with neural nets. IEEE ASSP Mag 4(2):4–22
38. Bouacha K, Yallese MA, Mabrouki T, Rigal J-F (2010) Statistical analysis of surface roughness and cutting forces using response surface methodology in hard turning of AISI 52100 bearing steel with CBN tool. Int J Refract Met Hard Mater 28(3):349–361
39. Sahoo AK, Rout AK, Das DK (2015) Response surface and artificial neural network prediction model and optimization for surface roughness in machining. Int J Ind Eng Comput 6(2):229
40. Azam M, Jahanzaib M, Wasim A, Hussain S (2015) Surface roughness modeling using RSM for HSLA steel by coated carbide tools. Int J Adv Manuf Technol 78(5–8):1031–1041
41. Basheer AC, Dabade UA, Joshi SS, Bhanuprasad V, Gadre V (2008) Modeling of surface roughness in precision machining of metal matrix composites using ANN. J Mater Process Technol 197(1):439–444
42. Aggarwal A, Singh H, Kumar P, Singh M (2008) Optimization of multiple quality characteristics for CNC turning under cryogenic cutting environment using desirability function. J Mater Process Technol 205(1):42–50